Infrared Absorption in Li-intercalated Tungsten Oxide

Anna-Lena Larsson [a], José Solis [b] jsolis@ipen.gob.pe, Gunnar Niklasson [a]

[a]Department of Engineering Sciences, The Ångström Laboratory, Uppsala University
P.O. Box 534, SE-75121 Uppsala, Sweden
[b]Instituto Peruano de Energía Nuclear, Av. Canadá 1470, Lima 41, Peru

Resumen

Películas delgadas amorfas y policristalinas de óxido de tungsteno fueron obtenidos por `sputtering` dc reactivo y películas nanocristalinas por evaporación avanzada. Los recubrimientos fueron sometidos a la intercalación de iones de Li antes de medir la reflectancia infrarroja. Para recubrimientos cristalinos la reflectancia en la región de 10-30 μm se incrementa después de la intercalación, indicando un incremento de la contribución de los electrones libres. Por otro lado, todos los recubrimientos muestran un incremento de la absorción para longitudes de onda menores que 10 μm cuando son intercaladas. La emitancia térmica puede variarse desde 0.5 hasta 0.7-0.75 por intercalación en recubrimientos con espesores mayores que 1 μm. La absorción e interferencia contribuyen al contraste de la emitancia.

Abstract

Thin films of amorphous and polycrystalline tungsten oxide, were produced by reactive dc magnetron sputtering and nanocrystalline films were deposited by advanced gas evaporation. The films were submitted to electrochemical intercalation of Li ions before infrared reflectance measurements were carried out. For crystalline films the reflectance in the wavelength region 10-30 μm increases upon intercalation, indicating an increasing free electron contribution. On the other hand, all the films display an increased absorption at wavelengths less than 10 μm when intercalated. The thermal emittance could be varied from about 0.5 to 0.7-0.75 by intercalation in films with thicknesses in excess of 1 μm. Both absorption and interference contribute to the emittance contrast.

1 Introduction

Electrochromic tungsten trioxide can be used for various applications, such as smart windows [1], rear-view mirrors [2,3], and gas sensors [4]. There is also an interest for tungsten trioxide as a coating with variable thermal emittance in order to achieve temperature control on spacecraft [5-8]. This is the intended application for the films investigated in this paper. Recently a number of innovative multilayer electrochromic variable emittance devices have been reported [8-11]. Polymer based devices [10] have appeared as the leading alternative to tungsten oxide based devices.

Li ions and charge-balancing electrons can be inserted into and extracted from a thin film of tungsten trioxide [1] by electrochemical techniques [12]. When the ions are intercalated (inserted) the films become absorbing and exhibit a blue colour. It is the change in the valence of the W atoms that gives rise to the optical modulation. Another way to obtain coloured films is to prepare them under conditions leading to oxygen deficiency, although, these films do not always exhibit complete bleaching [13]. In the infrared wavelength range some optical absorption modulation occurs as well. In addition, in variable emittance devices with multilayer configuration interference effects can be used to advantage for achieving a high infrared contrast [11].

In this paper we investigate the emittance modulation that can be obtained in single layers of tungsten oxide. The specific objective of this paper is to compare the infrared properties thin films of amorphous and polycrystalline WO_3 prepared by sputtering [14] and nanocrystalline WO_3 prepared by advanced gas evaporation [15]. An appreciable emittance variation upon intercalation requires film thicknesses in excess of 1 μm [16]. The crystallinity of the sputtered films can be increased by an elevated substrate temperature during deposition. The films produced in this way

are denoted "crystalline" and can exhibit upon intercalation a free-electron like reflectance modulation. The notation amorphous is used for films sputtered onto unheated substrates, which do not show any peaks in x-ray diffraction (XRD) measurements. The optical modulation of these films, when intercalated, is commonly described by theories of polaron absorption [18,19]. The films produced by the advanced gas evaporation technique consist of crystalline spherical nanoparticles. Diffraction peaks from the nanocrystalline films can be detected with XRD, but grain sizes are much smaller than for the sputtered crystalline films.

2 Experimental

Amorphous and crystalline tungsten trioxide films were deposited by reactive dc magnetron sputtering from a 5 cm diameter W (99.95%) target in an atmosphere of Ar (99.998%) and O_2 (99.998%), using a Balzers UTT 400 system. The power was 275 W, and the O_2/Ar flow ratio was 0.47. The sputter pressure was 30 mTorr and the background pressure was 10^{-4} mTorr. The substrate temperature was about 60 °C to 100 °C for the amorphous films and 350 °C for the crystalline ones. The substrate was glass covered with indium tin oxide (ITO), having a resistance/square of 15 Ω. Some samples subjected to X-ray diffraction measurements were deposited directly on glass substrates.

Nanocrystalline WO_3 films were deposited, using an Ultra Fine Particle Equipment, ULVAC Ltd., Japan. The substrate was glass covered with ITO with a resistance/square of 15 Ω. The surface of tungsten pellets (99.95%) was oxidized in 13 mbar synthetic air, in the evaporation chamber. Upon heating, the oxide sublimates into a vapour which condenses during cooling by the synthetic air, and small particles are formed. A small fraction of the particles are collected, and due to a pressure difference they are transported in a transfer pipe from the evaporation chamber into the deposition chamber. There the particles are deposited onto the substrate and a very porous film is grown. More information about the evaporation system and process can be found in Ref. [20].

The film thickness was measured in a Tencor AlphaStep instrument over a step formed by masking part of the substrate during deposition. Films with a number of thicknesses have been produced, but in this paper we focus on rather thick films in the range of 1 to 3 μm. The films were characterized by Rutherford Back-scattering Spectrometry (using alpha particles of energy 2 MeV backscattered at an angle of 166.1°) and Elastic Recoil Detection Analysis (using iodine ions of energy 21 MeV recoiled at an angle of 45°) in order to obtain the number of atoms per unit area. The density of the films were computed from the RBS and ERDA results together with film thicknesses and were found to be 5.60 g/cm^3, 6.44 g/cm^3 and 1.8 g/cm^3 for the amorphous, crystalline and nanocrystalline films, respectively. The as-deposited (asd) films were submitted to XRD using a Siemens D5000 diffractometer, with a CuKα cathode.

All films were intercalated in a liquid electrolyte consisting of 1 M $LiClO_4$ in propylene carbonate. The intercalation was carried out in an argon environment inside a glovebox, with controlled humidity of less than 4 ppm. A standard three-electrode set-up was used, together with an ECO Chemie Autolab potentiostat. The sample was used as the working electrode, while Li foils were used as counter and reference electrodes. All films were pre-cycled within the reversible intercalation range until they exhibited a stable electrochemical response. The optical measurements were done ex-situ, i.e. the intercalated samples were taken out of the glovebox and washed in ethanol before the measurements. This resulted in an average loss of inserted charge of 15 %, which was observed by comparing with the charge extracted from the films after each optical measurement. From the measured extracted charge, together with the film densities given above, the intercalation level, x (=Li/W ratio), was calculated. Specular reflectance spectra were taken at near normal incidence in a Perkin-Elmer 983 spectrophotometer in the wavelength range 2 to 50 μm. In the double beam configuration, gold mirrors were used as references for the sputtered films, and aluminium mirrors for the advanced gas evaporated film.

3 Results and Discussion

Figure 1 shows X-ray diffraction spectra for amorphous, crystalline and nanocrystalline tungsten oxide films. Amorphous films were obtained by sputtering at substrate temperatures below 200 °C. They show only a very broad hump, which can be attributed to the glass substrate. Polycrystalline films were obtained when the substrate temperature was above 300 °C. They exhibit a distinct diffraction pattern which indicates a monoclinic structure. The diffraction spectrum of the nanocrystalline films shows broader peaks and the structural determination is more difficult. Best agreement was found with the tetragonal structure, as shown by Solis et al. [20]. The grain size for the sputtered crystalline films was ~30 nm, as calculated from Scherrer's expression [21] and that for the nanocrystalline films was ~6 nm [20].

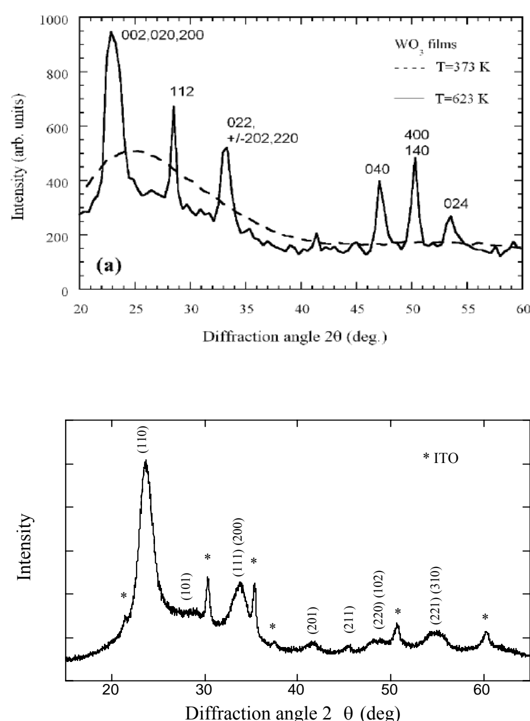

Figure 1. (a) X-ray diffraction spectra for amorphous and crystalline tungsten oxide films. The films were deposited by sputtering onto glass at the shown substrate temperatures. The indexed peaks are those of the monoclinic structure of WO_3. (b) X-ray diffraction spectrum for a nanocrystalline film deposited on indium-tin oxide (ITO) coated glass. The stars indicate peaks due to the ITO. The remaining peaks are indexed according to the tetragonal structure of WO_3.

The reflectance spectra, in the wavelength range from 2 to 50 μm, for a 1.45 μm thick sputtered amorphous film at different intercalation levels, can be seen in Fig 2a,b. The spectra show an oscillatory character due to interference effects. The TO phonon absorption (Reststrahlen band) is visible at about 15-20 μm. The oscillations shift towards longer wavelengths with increasing x, indicating that the refractive index increases with x. There also seems to be an increased absorption as x increases, as seen by the lowered reflectance level in the mid-infrared region and the damping of the interference oscillations [22]. An absorption band due to O-H-stretching modes can be seen at 3 μm in the unintercalated film, as well as a dip at 6 μm that arises from H-O-H vibrations. It has a narrower shape than the former one, and becomes smoothed out for x ≈ 0.17.

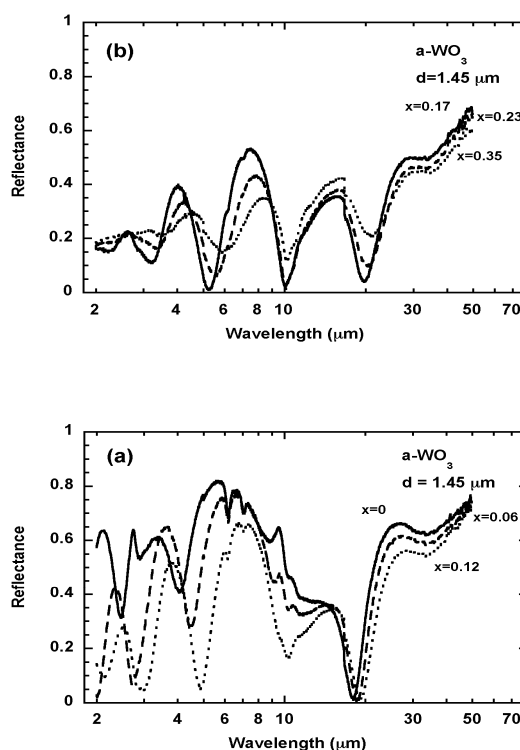

Figure 2. Reflectance as a function of wavelength for amorphous sputtered WO_3 at different intercalation levels, x, (a) x=0 (full line), x=0.06 (dashed), x=0.12 (dotted) and (b) x=0.17 (full line), x=0.23 (dashed), x=0.35 (dotted). The film thickness was 1.45 μm.

Fig. 3a,b shows reflectance spectra in the wavelength range 2 to 50 μm, for

nanocrystalline films produced by advanced gas evaporation. The figure shows spectra for the fully intercalated and deintercalated state. The interference oscillations are more damped than in fig. 2. Again we see absorption peaks at 3 and 6 μm as discussed above, and their strength also decreases upon intercalation. The absorption at 10-25 μm is due to the Reststrahlen band of tungsten oxide.

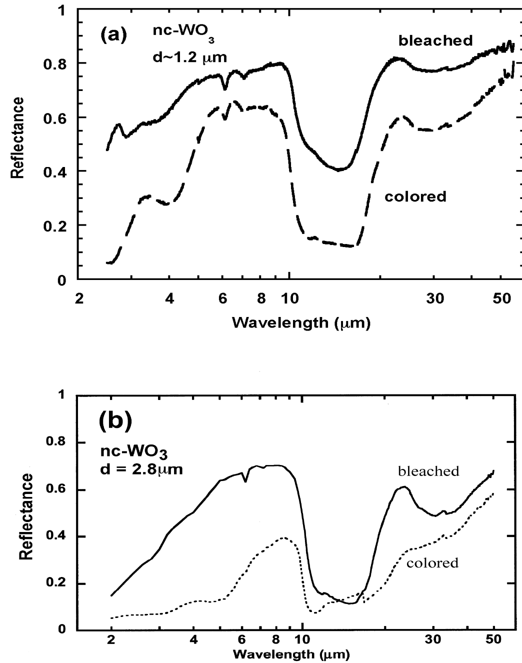

Figure 3. Reflectance for nanocrystalline WO_3 produced by advanced gas deposition, for the deintercalated (bleached, x=0) and intercalated (colored, x=0.36) states. The film thicknesses were about (a) 1.2 μm and (b) 2.8 μm

The reflectance of a crystalline tungsten oxide film at different intercalation levels is shown in Fig. 4a,b. Interference effects are prominent for low values of x. For x ≥ 0.14 the reflectance of the crystalline film increases and gradually becomes more featureless. Interference effects and phonon absorption are being washed out. This is a clear indication of free-electron like behaviour, i.e. electrons are now inserted into extended states in the conduction band.

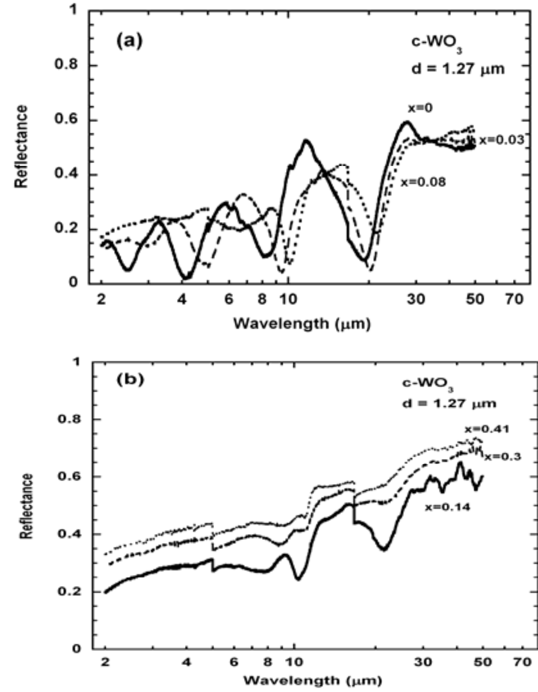

Figure 4. Reflectance as a function of wavelength for a crystalline sputtered WO_3 film at different intercalation levels, x, (a) x=0 (full line), x=0.03 (dashed), x=0.08 (dotted) and (b) x=0.14 (full line), x=0.3 (dashed), x=0.41 (dotted).

We now discuss the contributions to the variation of the infrared response upon intercalation. The Reststrahlen band centered at 15-20 μm is prominent in all the spectra, but its shape varies considerably. The shape is probably influenced both by interference effects and variations of the microstructure of the films. For the crystalline films at high intercalation levels (fig. 4b), the Reststrahlen band is almost not seen, because of the increased free electron contribution. The measured spectra also exhibit considerable changes in the wavelength region below 10 μm. In order to distinguish interference effects from absorption in this region, we have estimated the optical constants from the envelopes of the interference fringes, using the method of Kushev *et al.* [23]. Because of the few visible fringes, making an evaluation of the wavelength dependence uncertain, we carried out the evaluation for a single wavelength of about 5 μm. It was shown that the absorption coefficient, α always increased with the intercalation level, x, demonstrating the importance of absorption modulation in this region. The amorphous films were the

least absorbing with $\alpha=1.2\ 10^5\ m^{-1}$ for x=0, and increasing to $4.4\ 10^5\ m^{-1}$ for x=0.12 and $1.3\ 10^6\ m^{-1}$ for x=0.35. The crystalline films exhibited a higher absorption coefficient: $\alpha=1.1\ 10^6\ m^{-1}$ for x=0 and $1.8\ 10^6\ m^{-1}$ for x=0.14. In this latter case no evaluations were possible for higher x-values. The absorption coefficient for the nanocrystalline films is more uncertain, but in the intercalated state, it seems to be of the same order of magnitude as for the crystalline ones. The increasing mid-infrared absorption is most probably a consequence of the pronounced near infrared (NIR) absorption in intercalated films [18,20,24]. In the wavelength range between 2 μm and 10 μm, we are observing the low energy tail of the NIR absorption peak.

The thermal emittance was calculated from:

$$e = \frac{\int_{2\,\mu m}^{50\,\mu m} d\lambda (1 - R_\lambda) B_{T,\lambda}}{\int_{2\,\mu m}^{50\,\mu m} d\lambda B_{T,\lambda}} \quad , (1)$$

where the integrals are over the wavelength λ, R is the measured reflectance as a function of wavelength, and B is the wavelength and temperature dependent blackbody radiation [25]. It should be noted that our computed emittance values are approximate, since we only measured the specular reflectance at near-normal incidence. The computed emittance as a function of x is shown in Fig 5.

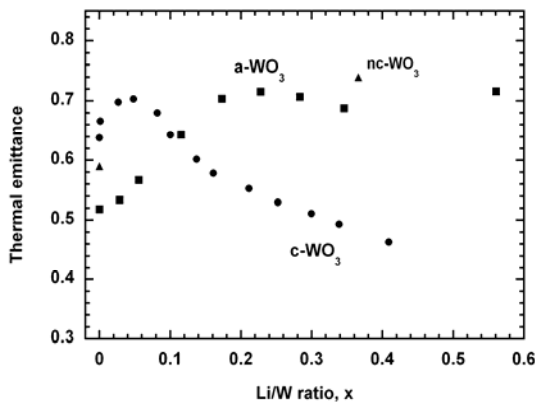

Figure 5. Emittance for crystalline (dots), amorphous (squares) and nanocrystalline (d=2.8 μm, triangles) WO_3 films, as a function of intercalation level (Li/W ratio), x.

It is seen that the emittance of the amorphous films increases with Li/W ratio. For the crystalline films, the emittance first increases up to x=0.05 and then decreases again, because of the increased reflectance at high x. The emittance modulation range for the sputtered amorphous and crystalline films is 0.52 to 0.72, and 0.70 to 0.49, respectively. For comparison, the corresponding emittance ranges for the nanocrystalline films in fig. 3a and 3b are 0.35 and 0.6 and 0.59 and 0.74, respectively. It can be seen that they exhibit a higher emittance in the intercalated state, with values similar to the amorphous films. However, for practical applications problems with substrate adherence and mechanical stability of these porous nanocrystalline films have to be overcome.

4 Conclusions

Thin films of amorphous and crystalline WO_3 were produced by reactive dc magnetron sputtering. Nanocrystalline WO_3 was produced by advanced gas deposition. The infrared specular reflectance was measured ex-situ at different stages of intercalation of Li into the films. The film microstructure exhibits a profound influence on the infrared-optical properties. The emittance of the amorphous and nanocrystalline films increases upon intercalation; hence they are more infrared absorbing when intercalated with Li. The crystalline films show the same trend at low intercalation levels, but for x>0.05 the emittance exhibits a pronounced decrease. This is seen as an increased reflectance, probably due to free-electron absorption from the inserted electrons. The tungsten oxide films exhibit a considerable emittance variation, and could be of interest in applications.

5 Acknowledgements

This work was financially supported by the Swedish National Space Board (SNSB) through the AME graduate program at Uppsala University, Sweden, and by the Swedish Research Council, the Swedish Foundation for Strategic Environmental Research (MISTRA) and the Swedish National Energy Administration. We are grateful to Göran Possnert and Alenka Razpet

for assistance with RBS and ERDA measurements.

6 References

[1] Granqvist CG. Handbook of Inorganic Electrochromic Materials. Amsterdam: Elsevier; 1995.

[2] Baucke FGK. Proceedings of the NATO Advanced Study Institute. Vol. C05, Marthinus Nijhoff, Dordrecht; 1985. p. 506.

[3] Shun-Hsiang H, Kuei-Hung C, Wen-Wei S. Light-responsive control device of electrochromic rearview mirror system. US Patent US2003122059; 2003.

[4] Madou MJ, Morrison SR. Chemical Sensing with Solid State Devices. San Diego: Academic; 1989.

[5] Hutchins MG, Ageorges P, Butt NS, Topping AJ. Energy. 1998; 15: 165.

[6] Hale JS, Woollam JA. Thin Solid Films. 1999; 339: 174.

[7] Bessiere A, Beluze L, Morcrette M, Lucas V, Viana B, Badot JC. Chem. Mater. 2003; 15: 2577.

[8] Franke EB, Trimble CL, Hale JS, Schubert M, Woollam JA. J. Appl. Phys. 2000; 88: 5777.

[9] Bessiere A, Marcel C, Morcrette M, Tarascon JM, Lucas V, Viana B, Baffier N. J. Appl. Phys. 2002; 91: 1589.

[10] Chandrasekhar P, Zay BJ, Birur GC, Rawal S, Pierson EA, Kauder L, Swanson T. Adv. Funct. Mater. 2002; 12: 95.

[11] Larsson AL, Niklasson GA. Mater. Lett. 2004; 58: 2517.

[12] Bard JB, Faulkner LR. Electrochemical Methods. New York: Wiley; 1980.

[13] Georg A, Graf W, Wittwer V. Sol. Energy Mater. Sol. Cells. 1998; 51: 353.

[14] Wasa K, Hayakawa S. Handbook of Sputter Depostiton. Park Ridge: Noyes; 1992.

[15] Hayashi C. Ultra-fine Particles. Westwood: Noyes; 1997.

[16] Larsson AL, Niklasson GA, Stenmark L. Proc. SPIE 4102. (2000) 69.

[17] Cogan SF, Plante TD, Parker MA, Rauh RD. J. Appl. Phys. 1986; 60: 2735.

[18] Berggren L, Azens A, Niklasson GA. J. Appl. Phys. 2001; 90: 1860.

[19] Calvani P. Riv. Nuovo Cimento 24. 2001; 1.

[20] Solis JL, Hoel A, Lantto V, Granqvist CG. J. Appl. Phys. 2001; 89: 2727.

[21] Cullity BD. Elements of X-ray Diffraction. Reading, MA: Addison-Wesley; 1956.

[22] Swanepoel R, Afr S. Tydskr. Fis. 12. 148; 1989.

[23] Kushev DB, Zheleva NN, Gyulmezov MI, Koparanova MH. Infrared Phys. 1993; 34: 163.

[24] Larsson AL, Sernelius B, Niklasson GA. Solid State Ionics. 2003; 165: 35.

[25] Wolfe WL, Zissis GJ. (Eds.). The Infrared Handbook. Office of Naval Research, Washington, DC, 1985.